
A Dual-Photopeak Window Method for Scatter Correction

M.A. King, G.J. Hademenos, and S.J. Glick

Department of Nuclear Medicine, University of Massachusetts Medical School, Worcester, Massachusetts

The imaging of scattered photons degrades contrast and is a major source of error in the quantitation of activity. It was hypothesized that, if the photopeak was divided into two nonoverlapping energy windows, a regression relation could be obtained between the ratio of counts within these windows and the scatter fraction for counts within the total region. This idea was tested by acquiring dual photopeak window acquisitions of a ^{99m}Tc point source in an elliptical attenuator, and at the same locations in air. From these, a regression between the scatter fraction and window ratio was determined. When this regression was applied to estimate the scatter distribution for acquisitions in both uniform and nonuniform elliptical attenuators, the residual scatter fraction was reduced approximately ten-fold and the estimated scatter line spread functions matched very closely the tails of the total line spread functions. In SPECT acquisitions, dual-photopeak window scatter correction was observed to significantly increase the contrast of "cold" spheres, improve the accuracy of estimating activity at the center of "hot" spheres, and return the three-dimensional modulation transfer function for point sources in an elliptical attenuator to near their in-air shape.

J Nucl Med 1992;33:605-612

The inclusion of events from scattered photons in emission images degrades the contrast of lesions and hence their detection, and biases the quantitation of activity (1). A number of scatter compensation techniques have been developed for use with NaI(Tl) based gamma cameras and tomographic reconstruction by filtered backprojection. These include: (1) decreasing the values of the linear attenuation coefficient used with attenuation correction to account for the imaging of the additional scattered photons (1,2); (2) use of an average scatter fraction (SF) to numerically correct for scatter (1); (3) use of convolution methods to estimate the amount and spatial distribution of scatter which is then subtracted from the emission image to yield scatter compensation (1,3-12); (4) use of an asymmetric energy window to decrease the amount of scatter imaged (1,13); (5) subtraction of the scaled counts

per pixel within a second or "scatter" energy window (i.e., "k" times scatter image) from the counts in each pixel for the photopeak window (1,7,10,12,14,15); (6) holospectral imaging (16); (7) energy-weighted acquisition of scintigraphic images (17); and (8) prediction of the counts due to scatter at each spatial location based on an analysis of the energy spectrum detected for that location (18-20). Each of these methods has its limitations. The use of an effective linear attenuation coefficient or an effective SF does not restore the contrast lost by imaging scatter and only numerically compensates for scatter to the extent of how accurate an approximation they are. The convolution methods address both loss of contrast and alteration in the number of events detected; however, these methods are typically applied using one or two approximations to the scatter distribution which are assumed to hold throughout the medium. The scatter response function and system modulation transfer function (MTF) have been shown to be nonstationary, especially near the sides of the attenuator (3,6,8-11,21). With asymmetric energy windows, the number of counts collected is reduced thus elevating noise, and scatter is still present, although at a reduced level (13). The scaling factor used with the dual-window subtraction method varies with source geometry, and the estimated scatter distribution from the lower energy window is not of exactly the same shape as the scatter distribution within the photopeak window (7,10,15). Holospectral imaging requires the acquisition of multiple (16 to 32) images of each view in order that the energy spectrum of each pixel may be defined, and it has not been proven that the separation obtained actually does compensate for scatter (16). The 5x5 finite impulse response filter used to do the energy-weighted correction is much smaller in spatial extent than the scatter tails (17). The methods which analyze the local energy spectrum estimate the spatial variation in the scatter within the photopeak window without the need for using a scaling factor (18,19). The drawbacks of these methods are again, the need for a number of energy windows and the influence of noise on the estimation of scatter. Thus, no scatter correction method has been adopted as the standard method for clinical use.

The basis for the dual-photopeak window (DPW) method of scatter correction proposed herein is that Compton scattered photons contribute more to the lower energy portion of the photopeak than the high energy side (1,10,

Received Jul. 23, 1991; revision accepted Nov. 6, 1991.
For reprints contact: Michael A. King, PhD, Department of Nuclear Medicine, University of Massachusetts Medical Center, 55 Lake Avenue North, Worcester, MA 01655.

13,18,22-24). It was therefore hypothesized that, if the photopeak region was divided into two nonoverlapping energy windows, a regression relation could be obtained between the ratio of counts within these windows and the scatter fraction for the counts within the total photopeak window. This method would allow the estimation of the scatter distribution within the photopeak window with the use of only two energy windows and without the use of arbitrary scaling factors. Its use would only require that calibration studies be performed to determine the regression coefficients for a given system and pair of energy windows. It therefore could be easily implemented on any modern camera that allows simultaneous acquisition from two abutted energy windows. The idea is, in some ways, similar to that of another group (20). They, however, assumed a constant shape which scales with changes in the scatter fraction for the distribution of scatter within the energy spectrum. This allowed them to define the location of two energy windows so that the amount of scatter in each window was the same. Scatter correction was performed by subtracting the counts of the lower window from the upper window. This, on average, corrects for scatter if the assumptions and window specifications are correct. It also results in a loss of primary counts since the lower window contains primary as well as scatter and therefore biases quantitation and increases image noise.

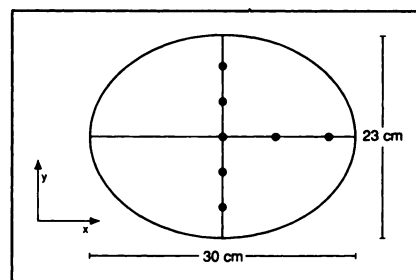
This paper first describes the calibration study that must be performed to obtain the regression coefficients. It then details how the method is applied to yield scatter correction. Next, the problem of camera nonuniformity is discussed and how the method is modified to account for it. Finally, the method is tested in terms of its ability to reduce the scatter fraction of point sources, match the shape of the "tails" of line spread functions (LSFs), return the MTF of points acquired in a scattering medium to near their in-air (or no scatter) shape, and improve the accuracy of activity quantitation at the center of spheres in SPECT acquisitions.

METHODS

Calibration Study

To obtain the regression relation between the window ratio and scatter fraction (SF), a point source of ^{99m}Tc was imaged in a 30×23 cm, elliptical cross-sectional, tub phantom which was 50 cm in height. The activity of the ^{99m}Tc point source was initially 18 MBq (0.5 mCi), and the point source consisted of a small amount (2 mm length) of concentrated ^{99m}Tc solution at the end of a 30-cm long, 1 mm inner diameter, glass tube. The phantom was imaged with the point source at five depths along its minor axis as shown in Figure 1. The phantom was positioned with its nearest surface 10 cm from the face of the low-energy, high-resolution, parallel-hole collimator of the camera. A single-head, circular field of view, SPECT camera (Dyna-scan, Picker International, Cleveland, OH) was employed. Images were collected for each of two 10% windows that together cover the standard 20% symmetric energy window used for imaging (Fig. 2). The images were recorded on a standard nuclear medicine

FIGURE 1. Cross-sectional view of 30×23 cm elliptical phantom geometry. The phantom was imaged from the top. The dots on the axis show the locations at which point source acquisitions were performed.



computer system (PCS-512, Picker International, Cleveland, OH). This computer system was also used for DPW correction of the images and data analysis. Images of the same point source in air at the same locations imaged in the phantom were obtained for use in calculating the SF. The total counts within each of the energy windows for the point source in the phantom, and in air, were corrected for background, acquisition time, physical decay, and attenuation (sources in phantom only), and used to calculate the SF (21,25). A regression relation between SF and the ratio of the corrected counts in the lower window divided by the upper window (R_s) for points sources in a scattering medium of the form:

$$SF = A \cdot R_s^B + C \quad \text{Eq. 1}$$

was obtained through use of a nonlinear, least-squares, fitting routine (26). For the five point sources along the minor axis, values of A, B and C were 0.32, 1.9 and -0.15 , respectively, with a correlation coefficient of 0.99.

Scatter Correction

With the regression relation determined by the calibration procedure, scatter correction was performed as follows. First, the ratio of the counts between the lower and upper windows at each pixel i, j is used as input to Equation 1 to obtain an estimate of the SF for each pixel. If there are no counts in the upper window, a ratio of infinity would result. Thus, when the counts in the upper window are zero, the ratio is set to a large value. From the pixel scatter fraction [SF(i, j)], the scatter-to-total ratio for each pixel [STR(i, j)] is estimated as:

$$STR(i, j) = SF(i, j) / [SF(i, j) + 1]. \quad \text{Eq. 2}$$

The STR(i, j) is then multiplied times the total number of counts corrected for decay, background, and acquisition time in both

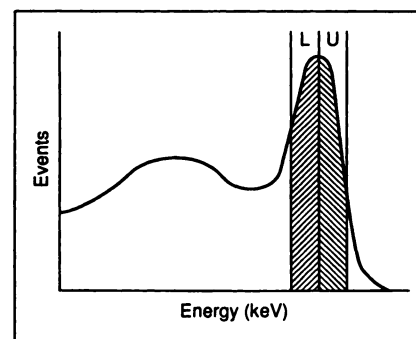


FIGURE 2. Typical energy spectrum showing location of lower (L) and upper (U) windows used with dual-photopeak window imaging.

windows [TC(i, j)] to give a pixel-by-pixel estimate of the scatter distribution [ES(i, j)] as:

$$ES(i, j) = STR(i, j) \cdot TC(i, j). \quad \text{Eq. 3}$$

Since the number of counts for a given pixel within each window is usually low, the ratio of these counts [R_S(i, j)] and, hence, the estimated scatter distribution is quite noisy. Therefore, the estimated scatter distribution is low-pass filtered before being subtracted from the total number of counts in the pair of windows for each pixel to yield the scatter corrected image as:

$$EP(i, j) = TC(i, j) - ES_{LP}(i, j), \quad \text{Eq. 4}$$

where ES_{LP}(i, j) is the low-pass filtered scatter estimate and EP(i, j) is the estimated primary photon image. The spatial distribution of scatter for an image is a highly blurred version of the primary image. That is, the MTF for scatter decreases much more rapidly than that of the primary (5,27). Thus, the high frequency portion of the DPW estimated scatter distribution can be eliminated without significantly biasing the scatter estimate. The filter used herein was a two-dimensional symmetrical Butterworth filter with a cutoff frequency equal to one-half the Nyquist frequency and an order of 4.0 (28). Optimization of the design of this filter is the subject of further investigations. This filtering is required to reduce the increase in pixel noise, caused by the subtraction of the scatter estimate in Equation 4.

Camera Uniformity

As formulated thus far, for the DPW method to be accurate, the only significant cause of variation in the window ratio should be scatter. Thus, the ratio of the counts between the two windows in the absence of scatter should be constant across the detection area, and not vary with head orientation for a given location. To investigate if these conditions could be met with the SPECT system used in this study, the following tests were performed. A 7-MBq (0.2 mCi) point source of ^{99m}Tc was imaged at a distance of 100 cm from the uncollimated face of the camera with head orientations of 0°, 90°, 180° and 270° with respect to having the camera facing the floor. Approximately 20 million counts were acquired at each angle for each window. The pixel by pixel ratio R_A for the point source acquisitions in air was calculated for each angle, and its variation with pixel location and head orientation were studied visually in images made from the R_{AS}. It should be noted that the uniformity test being performed herein is sensitive to both variation in energy spectrum and camera nonlinearity.

Investigation of Performance

The performance of DPW in correcting for scatter in point source acquisitions in a uniform medium was investigated using a source positioned at the seven locations within the elliptical cross-sectional phantom shown in Figure 1. The acquisitions were performed as detailed in the calibration section above.

Acquisitions of the same point source at comparable locations in air were also performed to allow calculation of the SF. The SF for the total window (sum of the pair of DPW windows), with and without DPW correction was calculated for each point. In addition, the images were summed along the horizontal axis, yielding plots of pseudo LSFs (10). These LSFs for the original and estimated scatter distribution were then plotted on the same axes to allow comparison.

An investigation of DPW correction of point source acquisitions in a nonuniform attenuating (scattering) medium was also conducted. This was done by including two "lung" shaped sty-

foam blocks (density of 0.02 g/cm³) into the elliptical cross-sectional phantom. The locations of the point sources studied with this geometry were at the center of the phantom, and at the two locations along the major axis indicated in Figure 5. The first of these two locations was at the center of one of the "lungs," and the second was just outside the "lung." SFs with and without DPW correction were determined, and a graphical comparison of the total and estimated scatter LSF's was performed.

The use of DPW correction coupled with SPECT imaging was assessed by acquiring 128 angle SPECT acquisitions of a point source at each of the three locations of Figure 1 along the major axis and at the same location in air. The original and DPW-corrected projection images were reconstructed using filtered backprojection and Bellini's intrinsic method of attenuation correction (29,30). A simple model for photon attenuation was employed (31). For the cases without and with DPW correction, the transmitted fractions (TFs) for the point source locations along the minor axis of the phantom (see Fig. 1) were fit by:

$$TF(x) = B_0 \exp(-u_E x), \quad \text{Eq. 5}$$

where x is depth, B₀ is the buildup factor at the surface of the attenuator, and u_E is the effective attenuation coefficient. For no scatter correction, B₀ was 1.12 and u_E was 0.11. With DPW correction, B₀ was 1.04 and u_E was 0.15. The parameters of the model were obtained by regression analysis using the data from the acquisitions of the point sources used in the calibration studies. The reconstructions of the point source in air were performed without attenuation correction. The three-dimensional MTFs of these acquisitions were then determined and a graphical comparison was made between the three-dimensional MTFs from point sources acquired at the same locations in air and in the scattering medium to determine the success of scatter correction.

The use of DPW correction of extended source distributions with SPECT imaging was performed by acquiring five DPW acquisitions from a SPECT phantom (Deluxe SPECT Phantom, Data Spectrum, Chapel Hill, NC). A 1.5 magnification was used, resulting in a voxel size of 0.39 cm per side, and a 16-cm radius of rotation was employed. The acquisition images were two dimensionally filtered with a Butterworth filter with order 4 and cutoff frequency equal to one-half the Nyquist frequency. These studies were then reconstructed and attenuation corrected as described above, and then the image contrast for the voxel which was visually at the center of the 3.2, 2.5, and 1.9 diameter spheres was calculated. The average number of counts per slice in the attenuation-corrected slices was approximately 400,000 for a one voxel wide slice. Visual comparison of slice uniformity with and without DPW correction was also performed.

An investigation of the accuracy of activity quantitation with SPECT imaging which results with use of DPW scatter correction was conducted as follows. DPW SPECT acquisitions of a 4.8 cm inner diameter sphere containing a known concentration of ^{99m}Tc [initially 9.3 MBq/ml (0.25 mCi/ml)] were obtained with the sphere at the center, and at one-fourth, one-half, and three-fourths the distance along the major axis of the elliptical tub phantom. The water in the tub contained no added activity. The ^{99m}Tc concentration in the sphere was decay corrected to the start of each acquisition. Prior to reconstruction, the counts in each frame were corrected for background and decay-corrected to the start of acquisition for that study. The frames from each of the pair of windows were summed with and without DPW correction. The

acquisitions were reconstructed by filtered backprojection using Bellini's method of attenuation correction (29,30) and the simple transmission model for photon attenuation (31). A 27-point (3×3×3) binomial smoothing filter was used to determine the counts at the center of each sphere. These counts multiplied by 100% were divided by the expected number of counts which would have been obtained from a point source in air whose activity was equal to that contained in a single voxel (31). This yielded the percent of air sensitivity which was used to assess the accuracy of activity quantitation.

RESULTS

Camera Uniformity

The ratio of the lower to upper window (R_A) for point sources in air was found to vary systematically across the flood field in conjunction with the location of the PMTs (Fig. 3). Therefore, the actual ratio used in the regression relation of Equation 1 for determining the regression coefficients and when applied to calculate scatter distributions (R_C) was

$$R_C(i, j) = R_S(i, j)/R_A(i, j), \quad \text{Eq. 6}$$

where R_S is the ratio in the scattering medium and R_A is the ratio for point sources in air. Thus, in actual application, R_S is calculated for each pixel from the dual-window acquisition, and these values are then divided by R_A for each pixel calculated from point source flood acquisitions performed on the same day.

The R_A map was observed to be a significant function of head angle for one small location at the edge of the field of view (Fig. 3). This appears to be due to the influence of gravity upon one PMT (32). At other locations, there were small regional shifts which varied maximally 5% in R_A between orientations. Thus, except for the region at the edge of the field of view, which was not used in the following phantom studies, the system was deemed suitable

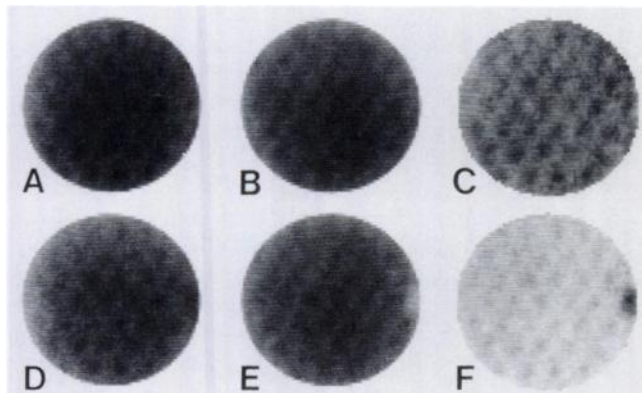


FIGURE 3. Intrinsic flood images for a ^{99m}Tc point source fixed 100 cm in front of the camera. (A) Lower window for camera facing down; (B) upper window for camera facing down; (C) ratio of lower to upper window for camera facing down; (D) lower window for camera facing up; (E) upper window for camera facing up; and (F) ratio of lower to upper windows for camera facing up.

for prototype testing of the DPW scatter correction method.

Scatter Fraction and LSFs for Uniform Attenuation Medium

Using regression coefficients obtained from the total counts for the five point source locations along the minor axis of the elliptical tub phantom, DPW scatter correction was applied on a pixel by pixel basis to the acquisitions of a ^{99m}Tc point source at each of the seven locations shown in Figure 1. The SF before and after DPW correction of these acquisitions are given in Table 1. Notice the nearly complete compensation for scatter with DPW correction, and that the method seems to work even for the points source locations moved laterally from being centered along the minor axis. Figure 4 shows the excellent agreement, both with variation in depth and lateral shifting of the source, between the estimated scatter LSFs and the tails of the total LSFs from these acquisitions. In these plots, the true scatter distribution is unknown, but with the near complete quantitative correction of scatter (Table 1) and the matching of the tails of the LSFs, it is likely that DPW is providing an excellent estimate of the scatter distribution.

Scatter Fractions and LSFs for Nonuniform Attenuation Medium

Using the same set of regression coefficients as above, DPW scatter correction was applied to the acquisitions of the ^{99m}Tc point source at each of the three locations in the "chest" phantom shown in Figure 5A. Again, a decrease in the SF to near zero was observed with DPW correction (Table 1), and an excellent matching of the scatter estimate with the tails of the LSF was observed (Fig. 5B–D). Thus, there seems to be evidence that one regression relation may be employed for both uniform and nonuniform attenuating mediums.

Comparison of Three-Dimensional MTFs

Figure 6 shows the x-axis of the three-dimensional MTF of the point source at each of the three lateral locations

TABLE 1
Scatter Fraction Versus Position in Elliptical Tub Phantom of Figure 1

Phantom geometry	Location	SF with no scatter correction	SF with DPW scatter correction
Uniform Medium	3.5 cm deep	0.27	0.00
	7.5 cm deep	0.47	0.01
	11.5 cm deep	0.63	0.01
	15.5 cm deep	0.80	0.04
	19.5 cm deep	0.92	0.05
	6.0 cm lateral	0.55	0.00
	12.0 cm lateral	0.36	-0.05
"Chest" Phantom	11.5 cm deep	0.72	0.05
	6.0 cm lateral	0.45	0.02
	12.0 cm lateral	0.48	0.05

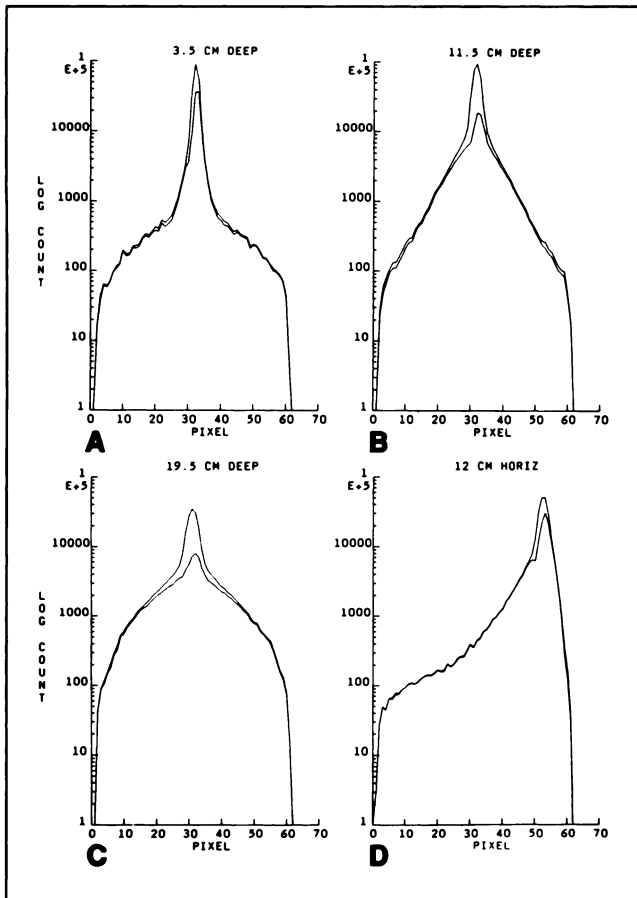


FIGURE 4. Semilogarithmic plots of total (upper line) and estimated scatter (lower line) counts in line spread functions versus pixel location for a ^{99m}Tc point source in the elliptical attenuator with uniform attenuation. Point source locations are: (A) 3.5 cm from top along minor axis; (B) 11.5 cm from top along minor axis; (C) 19.5 cm from top along minor axis, and (D) 12 cm lateral from center along major axis.

along the major axis of the phantom, or at equivalent locations in air. In comparing the in-air MTFs to those for the point source in the phantom and reconstructed without DPW correction, a significant drop in the MTFs at a low spatial frequency can be noted (5,27). It can also be noted that this low frequency degradation is in large part corrected by DPW scatter compensation prior to reconstruction.

Contrast of "Cold" Spheres

It can be seen in Table 2 that DPW correction provides a statistically significant improvement in contrast at the center of the spheres in the SPECT acquisitions of the Data Spectrum phantom. This is illustrated in Figure 7, which shows a slice through the center of the spheres reconstructed with and without DPW scatter correction. Notice that along with the increased contrast is an increase in the noise level of the slice. When 12×12 pixel regions of interests were placed over a "uniform" section of the phantom, an average (s.d.) of 10.5 (2.2) for the percent

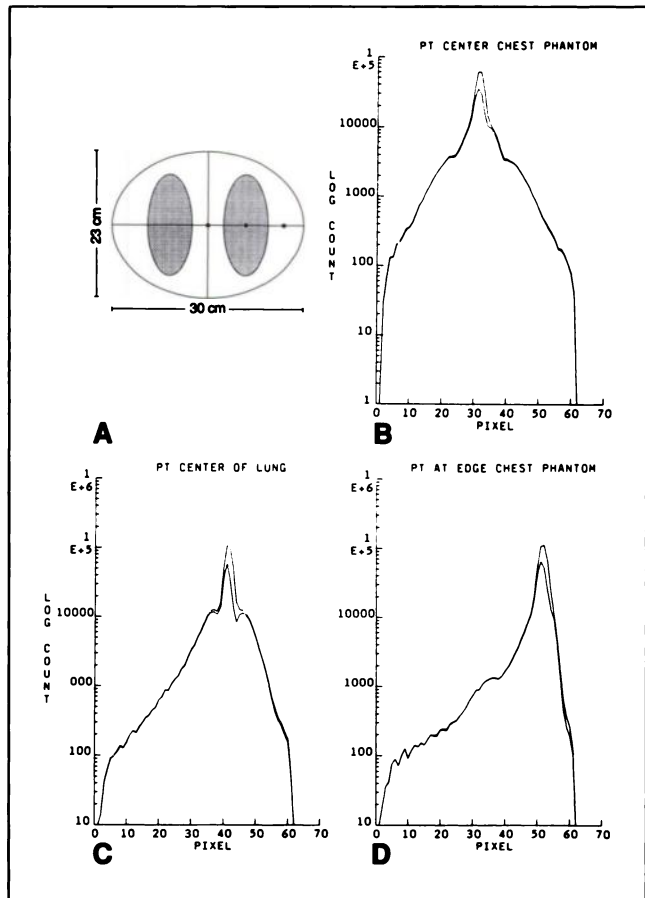


FIGURE 5. Geometry of point source acquisitions in nonuniform "chest" phantom (A), and semilogarithmic plots of total (upper line) and estimated scatter (lower line) counts in line spread functions versus pixel location for a ^{99m}Tc point source at indicated locations: (B) center of phantom; (C) center of right "lung"; and (D) 12 cm lateral from center along major axis.

fractional standard deviation was observed in the slices with no scatter correction, and a 13.9 (2.6) percent fractional standard deviation was observed in the slices with DPW correction. A slight increase in the contrast of uniformity defects is also noted; but no DPW-induced artifacts were seen.

Accuracy of Activity Quantitation

Table 3 provides a comparison between the percent of air sensitivity at the center of 4.8 cm diameter spheres filled with a ^{99m}Tc concentration when imaged individually at each of four locations in the elliptical phantom. Notice that DPW scatter correction combined with Bellini's method of attenuation correction (29), which uses a simple transmission model for photon attenuation (31), results in percent air sensitivities which are within 10% of the true value independent of location in the elliptical attenuator.

DISCUSSION

The DPW scatter correction method has been determined to decrease the SF by approximately ten-fold, pro-

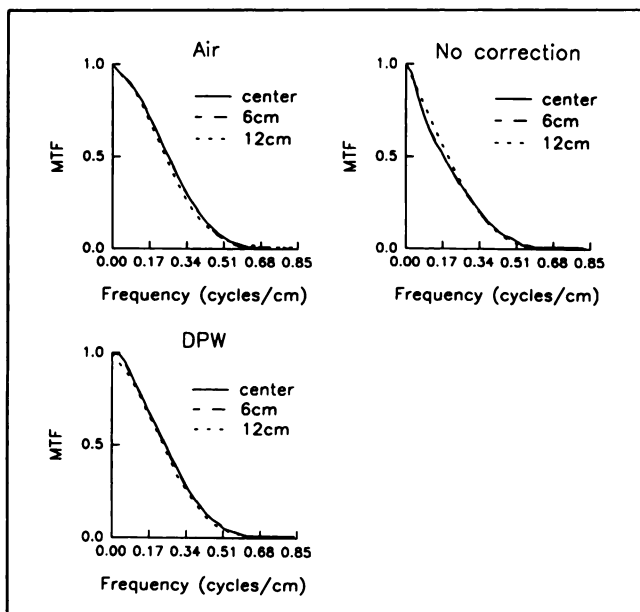


FIGURE 6. Plots of MTF along the x-axis for points at the center, 6 cm lateral, and 12 cm lateral in the 30×23 cm tub phantom with no scatter correction or with DPW correction, and at the same location in air.

duce estimated scatter LSFs that match the shape of the tails of the total LSF independent of depth, lateral displacement, or alterations in attenuating medium, to restore the post-reconstruction MTF to near its “in-air” shape, to provide a statistically significant increase in the contrast of “cold” spheres, and to provide for approximately accurate quantitation of activity concentration at the center of spheres. It also does not require significant processing time to estimate the scatter distribution via the DPW method. Therefore, it seems reasonable that this method is an excellent candidate for routine clinical use in both planar and SPECT imaging. The method should be carefully evaluated before widespread clinical use since with the present ad hoc Butterworth filtering of the scatter estimate it does increase the noise in the slices, and enhance camera nonuniformities. Thus, this method may or may not lead to more false-positives.

In order to perform the DPW method, a camera system that can image with a pair of abutted energy windows that do not significantly change their energy spectrum with

TABLE 2
Average (s.d.) %Contrast Versus Sphere Size for Data Spectrum Phantom

Diameter	No scatter correction	DPW scatter correction
3.2 cm	89 (8)	96 (6)*
2.5 cm	67 (2)	81 (9)*
1.9 cm	38 (8)	45 (9)*

* Significantly different at a p value of 0.05 by paired t-test.

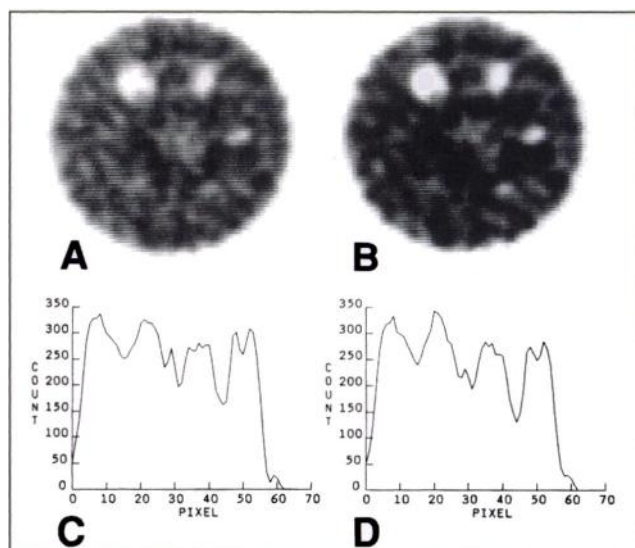


FIGURE 7. Slice through the center of the “cold” spheres: (A) with no scatter correction and (B) with DPW scatter correction. Count profiles through the slices at the level of the 1.9 cm sphere (row 33 of the images) are shown for (C) no scatter correction and (D) with DPW scatter correction.

head rotation (33) is required. Regional variation in energy spectrum can be compensated for by dividing the ratio of the pair of images obtained from the source(s) in a scattering medium by the ratio of the windows for a point source in air (i.e., using Equation 6). The use of the ratio of dual windows in the photopeak region is, in some ways, like using a fit to a Gaussian function to predict scatter (19). The “in-air” ratio is the distribution which should occur locally under low scatter conditions (initial Gaussian fit). As the amount of scatter increases, the number of counts in the lower window increases faster than the upper. This alters the ratio, and by the regression equation (Equation 1) the estimated SF. As the counts in the lower window continue to increase, the estimated SF increases. However, even if the SF should go to near infinity, the STR by Equation 2 would at most go to 1.0, indicating that all of the photons detected in the pixel should be considered scatter.

In Table 1 it can be seen that the measured scatter

TABLE 3
Percent of Air Sensitivity* for 27-Point, Binomial Weight Average at Center of 4.8-cm Diameter Sphere

Sphere location	No scatter correction	DPW scatter correction
Center	66.5	97.5
1/4	68.6	91.2
1/2	77.4	94.9
3/4	95.1	102.9

* cps/MBq of ^{99m}Tc at center of sphere times 100% and divided by cps/MBq of ^{99m}Tc for a point source at same location in air.

fraction with no correction at 11.5 cm deep in the uniform attenuating medium is less than that at 11.5 cm in the "chest" phantom. This difference may have been due to experimental error; however, the values in the table agree fairly well with those obtained via Monte Carlo simulations (34) of point sources at the same location in matching attenuation geometries (0.60 for uniform and 0.75 for "chest"). Thus, we hypothesize that the difference is real and may be due to the scatter accepted within the energy window being less attenuated by the "chest" geometry than in the uniform phantom.

A number of things still need to be investigated in terms of the application of DPW scatter compensation. First, a Monte Carlo comparison of DPW estimated and true scatter distributions, such as those performed for other methods (10). A preliminary investigation has been completed which agrees with the experimental studies reported here as to the potential usefulness of the DPW method (35). Monte Carlo simulations should also be used to investigate whether the regression equation varies with size and shape of the attenuator and density of the attenuating medium. Second, our choice of splitting the photopeak into two equal windows was arbitrary, and other combinations should be investigated. However, based on a preliminary investigation using Monte Carlo simulations (35), splitting the photopeak into two equal portions seems to be a good compromise between improved accuracy of scatter correction and sensitivity to noise. Third, for low count images, the scatter estimate is quite noisy. Further work on the design of low-pass filtering of this estimate is required. Fourth, the influence of changes in the local energy spectrum across the camera face, with camera rotation, with time at a given location (i.e., camera drift), and with counting rate (i.e., count pile-up) on the accuracy of the method, and what changes in the spectrum can be tolerated needs to be studied. It may be necessary to redo the calibration studies periodically to maintain the accuracy of the methods when camera electronic drift is present. This has not been a major factor for the SPECT system used here. The data reported in this paper were obtained over a 4-mo period using just a single calibration study at the start. Fifth, it should be investigated whether the DPW method can be extended to radionuclides such as ^{111}In and ^{201}Tl , which emit multiple energy photons. Finally, a study of the DPW's application to actual clinical images should be made.

ACKNOWLEDGMENTS

The authors would like to thank M.S. Rosenthal, PhD and B.C. Penney, PhD for many useful discussions regarding scatter correction. They would also like to thank the referees for their useful comments. This publication was supported by grant CA-42165 from the National Cancer Institute. Its contents are solely the responsibility of the authors and do not necessarily represent the official views of the National Cancer Institute. This manuscript is based on work presented, in part, at the 38th Annual

Meeting of the Society of Nuclear Medicine and published in abstract form as: King MA, Ljungberg M, Hademenos G, Glick SJ: A dual photopeak window method for scatter correction, *J Nucl Med* 1991;32:917.

REFERENCES

1. Jaszczak RJ, Floyd CE, Coleman RE. Scatter compensation techniques for SPECT. *IEEE Trans Nucl Sci* 1985;32:786-793.
2. Harris CC, Greer KL, Jaszczak RJ, Floyd CE, Fearnow EC, Coleman RE. Tc-99m attenuation coefficients in water-filled phantoms determined with gamma cameras. *Med Phys* 1984;11:681-685.
3. Axelsson B, Msaki P, Israelsson A. Subtraction of Compton-scattered photons in single-photon emission computerized tomography. *J Nucl Med* 1984;25:490-494.
4. Floyd CE, Jaszczak RJ, Greer KL, Coleman RE. Deconvolution of Compton scatter in SPECT. *J Nucl Med* 1985;26:403-408.
5. King MA, Schwinger RB, Penney BC, Doherty PW, Bianco JA. Digital restoration of indium-111 and iodine-123 SPECT images with optimized Metz filters. *J Nucl Med* 1986;27:1327-1336.
6. Msaki P, Axelsson B, Dahl CM, Larsson SA. Generalized scatter correction method in SPECT using point scatter distribution functions. *J Nucl Med* 1987;28:1861-1869.
7. Gilardi MC, Bettinardi V, Todd-Pokropek A, Milanese L, Fazio F. Assessment and comparison of three scatter correction techniques in single photon emission computed tomography. *J Nucl Med* 1988;29:1971-1979.
8. Msaki P, Axelsson B, Larsson SA. Some physical factors influencing the accuracy of convolution scatter correction in SPECT. *Phys Med Biol* 1989;34:283-298.
9. Frey EC, Tsui BMW. Parameterization of the scatter response function in SPECT imaging using Monte Carlo simulation. *IEEE Trans Nucl Sci* 1990;37:1308-1315.
10. Ljungberg M, Msaki P, Strand SE. Comparison of dual window and convolution scatter correction techniques using the Monte Carlo method. *Phys Med Biol* 1990;35:1099-1110.
11. Ljungberg M, Strand SE. Scatter and attenuation correction in SPECT using density maps and Monte Carlo simulated scatter functions. *J Nucl Med* 1990;31:1560-1567.
12. Yanch JC, Flower MA, Webb S. Improved quantification of radionuclide uptake using deconvolution and windowed subtraction techniques for scatter compensation in single photon emission computed tomography. *Med Phys* 1990;17:1011-1022.
13. Koral KF, Clinthorne NH, Rogers WL. Improving emission-computed tomography quantification by Compton-scatter rejection throughout offset windows. *Nucl Inst Meth Phys Res* 1986;A242:610-614.
14. Jaszczak RJ, Greer KL, Floyd CE, Harris CC, Coleman RE. Improved SPECT quantification using compensation for scattered photons. *J Nucl Med* 1984;25:893-900.
15. Koral KF, Swailen FM, Buchbinder S, Clinthorne NH, Rogers WL, Tsui BMW. SPECT dual-energy window Compton correction: scatter multiplier required for quantification. *J Nucl Med* 1990;31:90-98.
16. Gagnon D, Todd-Pokropek A, Arsneault A, Dupras G. Introduction to holospectral imaging in nuclear medicine for scatter subtraction. *IEEE Trans Med Imag* 1989;8:245-250.
17. DeVito RP, Hamill JJ, Treffert JD, Stoub EW. Energy-weighted acquisition of scintigraphic images using finite spatial filters. *J Nucl Med* 1989;30:2029-2035.
18. Koral KF, Wang X, Rogers WL, Clinthorne NH, Wang X. SPECT Compton-scattering correction by analysis of energy spectra. *J Nucl Med* 1988;29:195-202.
19. Rosenthal MS, Henry LJ. Evaluation and comparison of two scatter correction techniques [Abstract]. *J Nucl Med* 1990;31:873.
20. Logan KW, McFarland WD. Single photon scatter compensation by photopeak energy distribution analysis. *IEEE Trans Nucl Sci* 1991;1178-1182.
21. Coleman M, King MA, Glick SJ, Knesaurek K, Penney BC. Investigation of the stationarity of the modulation transfer function and the scatter fraction in conjugate view SPECT restoration filtering. *IEEE Trans Nucl Sci* 1989;36:969-972.
22. Floyd CE, Jaszczak RJ, Harris C, Coleman RE. Energy and spatial distribution of multiple order Compton scatter in SPECT: a Monte Carlo investigation. *Phys Med Biol* 1984;29:1217-1230.
23. Zasadny KR, Koral KF, Floyd CE, Jaszczak RJ. Measurement of Compton scattering in phantoms by germanium detector. *IEEE Trans Nucl Sci*

- 1990;37:642-646.
24. Rosenthal MS, Henry LJ. Scattering in uniform media. *Phys Med Biol* 1990;35:265-274.
 25. Manglos SH, Floyd CE, Jaszczak RJ, Greer KC, Harris CC, Coleman RE. Experimentally measured scatter fractions and energy spectra as a test of Monte Carlo simulations. *Phys Med Biol* 1987;22:335-343.
 26. Press WH, Flannery BP, Teukolsky SA, Vetterling WT. *Numerical recipes: the art of scientific computing*. New York: Cambridge A.P.; 1986:521-528.
 27. Sorenson JA, Phelps ME. *Physics in nuclear medicine*, second edition. Orlando: Grune and Stratton; 1987:372-375.
 28. Gonzalez RC, Wintz P. *Digital image processing*. Reading: Addison-Wesley; 1977:145-148.
 29. Bellini S, Piacentini M, Cafforio C. Compensation of tissue absorption in emission tomography. *IEEE Trans Acous Speech Sig Proc* 1979;27:213-218.
 30. Glick SJ, Hawkins WG, King MA, Penney BC, Soares EJ, Byrne C. Choice of intrinsic attenuation correction method and the three-dimensional modulation transfer function of SPECT. *Med Phys* 1992: in press.
 31. King MA, Glick SJ, Penney BC. Activity quantitation in SPECT: a comparison of three attenuation correction methods in combination with pre-reconstruction restoration filtering. *IEEE Trans Nucl Sci* 1991;38:755-760.
 32. Rogers WL, Clinthorne NH, Harkness BA, Koral KF, Keyes JW. Field-of-view requirements for emission computed tomography with an Auger camera. *J Nucl Med* 1982;23:166-168.
 33. Swailem FM, Koral KF, Rogers WL. Count-based monitoring of Anger-camera spectra-local energy shifts due to rotation. *Med Phys* 1991;18:565-567.
 34. Ljungberg M, Strand SE. A Monte Carlo program for the simulation of scintillation camera characteristics. *Comput Meth Progr Biomed* 1989;29:257-272.
 35. Hademenos GJ, Ljungberg M, King MA, Glick SJ. A Monte Carlo investigation of the dual photopeak window scatter correction method. *IEEE Trans Nucl Sci* 1992: submitted.

(continued from p. 580)

SELF-STUDY TEST

Pulmonary Nuclear Medicine

ANSWERS

secondary lymphoma or with infection due to *Mycobacterium tuberculosis* or *Mycobacterium avium-intracellulare*. Gallium accumulation associated with the lymphadenopathy of AIDS per se is usually of relatively mild intensity.

ITEM 4 Pulmonary Clearance of Radioaerosols

ANSWER: D

Numerous factors are important in determining the clearance rate of a radioaerosol from the lung. Major differences exist between the clearance rates and pathways of soluble and insoluble aerosols. Insoluble aerosols include those of particulate nature, such as ^{99m}Tc colloids or albumin particles, which must be cleared from the airways and alveoli by either mucociliary action or by lymphatic drainage. Mucociliary clearance requires several hours, even from relatively central airways, and lymphatic clearance of particulates can take days to weeks. On the other hand, soluble radioaerosols are cleared quickly by gaining direct access to the pulmonary blood supply across the alveolar-capillary membrane.

The clearance rates of various soluble aerosols are influenced by a number of factors, including the lipophilicity and polarity of the agent. In general, the more lipophilic and polar compounds are likely to be absorbed more rapidly. The molecular weight of a compound, however, also seems to have an influence. Some relatively high molecular weight

lipophilic compounds have slower pulmonary clearances than would be predicted from their lipid solubility alone.

Size is an important factor in radioaerosol clearance, whether the size refers to the molecular weight of a soluble compound, as mentioned above, or whether it refers to the physical size of the inhaled aerosol droplets. Larger aerosol droplets tend to deposit more centrally. From this central location, mucociliary clearance can act more effectively and quickly to clear the particles from the lungs. Conversely, if molecular size is considered, a larger compound may have a slower peripheral clearance. An agent with a combination of physical characteristics leading to the fastest clearance would have a relatively small molecular weight and be a polar, lipophilic compound delivered to the lung as a submicronic aerosol.

Alveolar-capillary membrane permeability appears to be a major factor in determining the clearance rate of soluble radioaerosols from the lung. The clearance of these compounds seems to be related far more closely to the available surface area for absorption across this membrane than to the pulmonary blood flow rate, itself. Total obstruction of pulmonary arterial flow to a lung leads to markedly diminished clearance of soluble radioaerosols, although a small amount of radioaerosol activity still may be absorbed through the bronchial circulation. However, within the typical range of pulmonary blood flow rates encountered in clinical practice, blood flow rate per se has relatively little influence on clearance rates.

For further in-depth information, refer to the syllabus pages in Nuclear Medicine Self-Study I.